高レイノルズ数壁乱流における微粒子の加速度統計に関する研究

辻　　義之　名古屋大学
山本　義暢　山梨大学
恒吉　達矢　名古屋大学

研究背景および目的

乱流中の微粒子（慣性粒子）運動の統計的性質

○乱流衝突モデルにおける凝集（クラスタリング）を特徴づける関数が、レイノルズ数依存性をもつことが明らかにされ、**雲物理の理解**が格段に進んでいる。

○高レイノルズ数の数値計算は、その制約から**一様等方な乱流場**を対象に実施される場合が多く、乱流衝突モデルにも一様等方性が暗に仮定されている。実際の気象乱流では、大きなスケールの非等方性が顕著となる。

○高レイノルズ数では、小さなスケールは大きなスケールの影響を受けずに一様等方な性質を満たす（局所等方性仮説）ことが期待されるが、微細粒子の運動が大きなスケールの**非一様性**の影響をどれくらい受けるか？

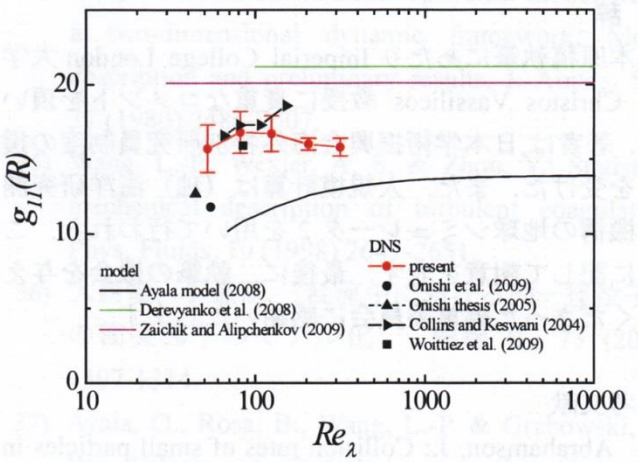

Fig. 6: Preliminary DNS results on RDF at contact for monodispersed droplets, $g_{11}(x=R_{11})$, with St=0.4. DNS results in literature[20,46,48,49] and model predictions[37,39,47] are also drawn.

[1] 大西　領、ながれ、vol.33, pp.241-245, (2014)
[2] 大西　領、高橋桂子、ながれ、vol.30, pp.385-394,(2011).

研究背景および目的

高レイノルズ数壁乱流における微粒子の加速度統計に関する研究

○大気乱流中の雨粒形成において、微粒子の衝突過程を理解することは、降雨予測の高精度化に不可欠となる。

○一様等方乱流中の微粒子の運動については多くの知見が得られているが、大気境界層など**せん断が支配的な流れ場**においては、その詳細は明らかにされていない。

○本研究では、壁乱流における高レイノルズ数乱流場の数値計算をおこない、**微粒子のラグランジュ加速度の統計性を局所等方性仮説を介して理解することを目的とする。**また、慣性粒子の可視化実験との対比から粒子衝突過程を検証し、雨粒の乱流衝突モデルの高精度化に資する。

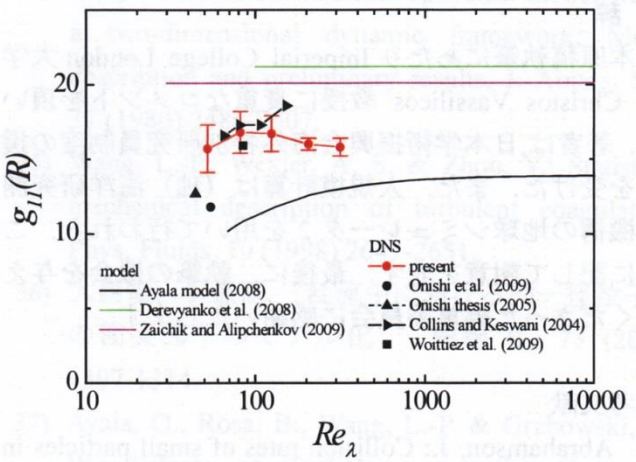

Fig. 6: Preliminary DNS results on RDF at contact for monodispersed droplets, $g_{11}(x=R_{11})$, with St=0.4. DNS results in literature[20,46,48,49] and model predictions[37,39,47] are also drawn.

[1] 大西　領、ながれ、vol.33, pp.241-245, (2014)
[2] 大西　領、高橋桂子、ながれ、vol.30, pp.385-394,(2011).

慣性粒子の加速度

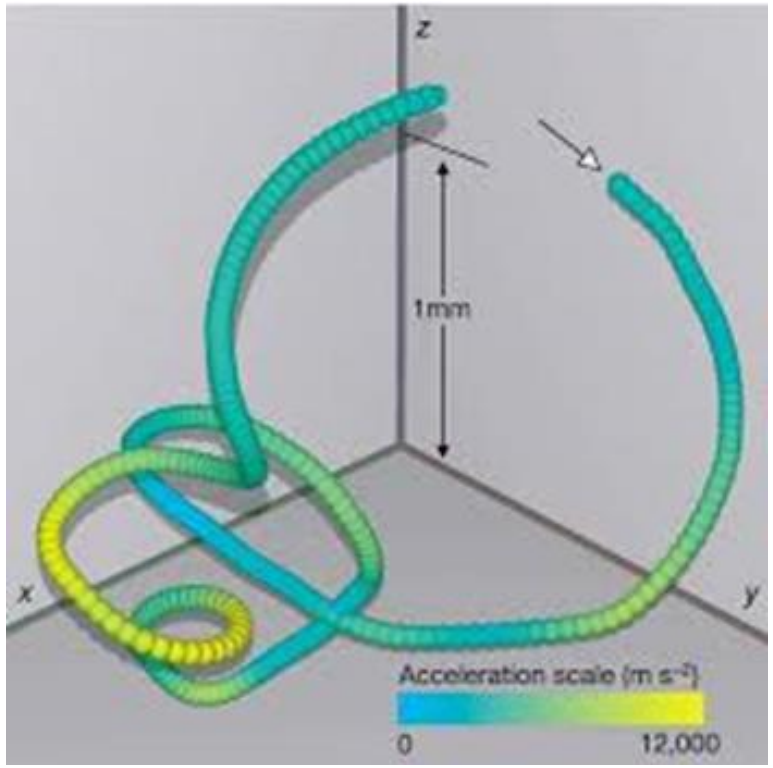

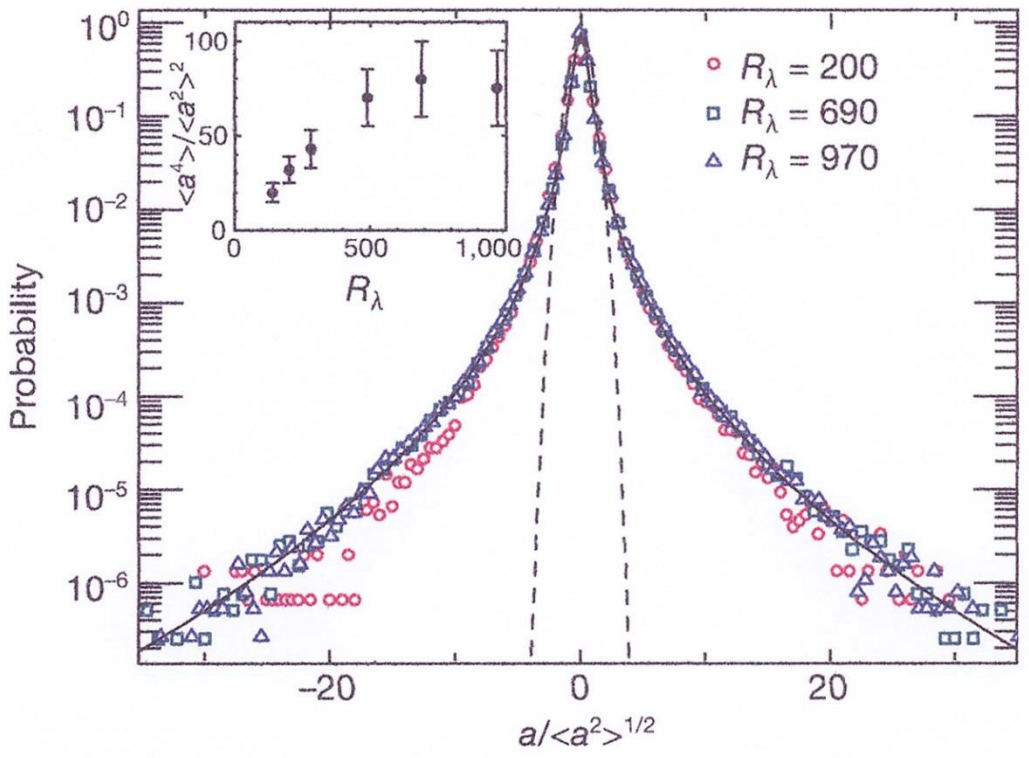

A. La Porta, G.A. Voth, A.M. Crawford, J. Alexander and E. Bodenschatz, Fluid particle accelerations in fully developed turbulence, **Nature (London) 409, 1017 (2001)**.

Observed particle acceleration is up to 1500 times the acceleration of gravity.

$$P(a) = C\exp\left\{-a^2\Big/\left(1+\left|\alpha\beta/\sigma\right|^{\gamma}\right)\sigma^2\right\}$$

Stretched exponential

$\sigma = 0.508 \quad \gamma = 1.588 \quad \beta = 0.539$

Acceleration in classical turbulence

Lagrangian acceleration of fluid particle is given as

$$\vec{a} = \frac{D\vec{u}}{Dt} = \frac{\partial \vec{u}}{\partial t} + (\vec{u} \cdot \nabla)\vec{u}$$

From the Navier-Stokes equation, Lagrangean acceleration of fluid particle is written as

$$\vec{a} = -\nabla(p/\rho) + \nu \nabla^2 \vec{u}$$

Acceleration is decomposed into the contribution from pressure gradient term and viscous force.

For incompressible homogeneous turbulence $\langle \nabla p \cdot \vec{u} \rangle = 0$ so that the above equation gives

$$\langle \vec{a} \cdot \vec{a} \rangle = \langle \nabla p' \cdot \nabla p' \rangle + \nu^2 \langle \nabla^2 \vec{u} \cdot \nabla^2 \vec{u} \rangle \quad , \qquad p' = (p/\rho)$$

Acceleration in classical turbulence

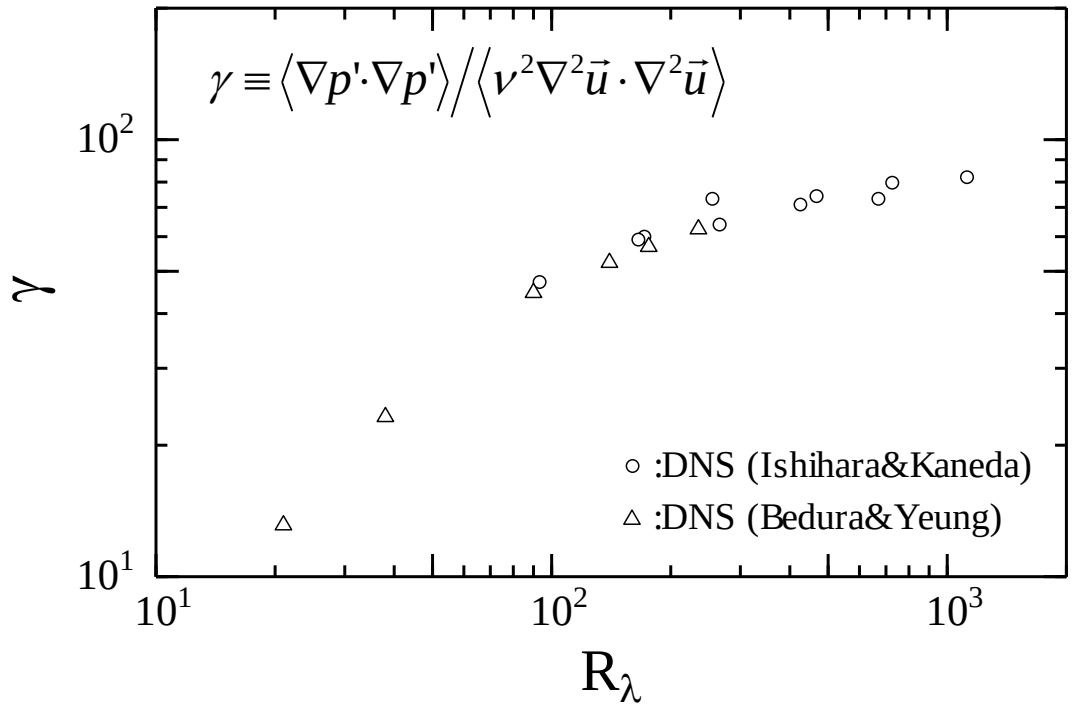

$$\langle \vec{a} \cdot \vec{a} \rangle = \langle \nabla p' \cdot \nabla p' \rangle + \nu^2 \langle \nabla^2 \vec{u} \cdot \nabla^2 \vec{u} \rangle \approx \langle \nabla p' \cdot \nabla p' \rangle$$

In fully developed turbulence, the viscous dumping term is small compared with the pressure gradient term.

High acceleration event in classical turbulence

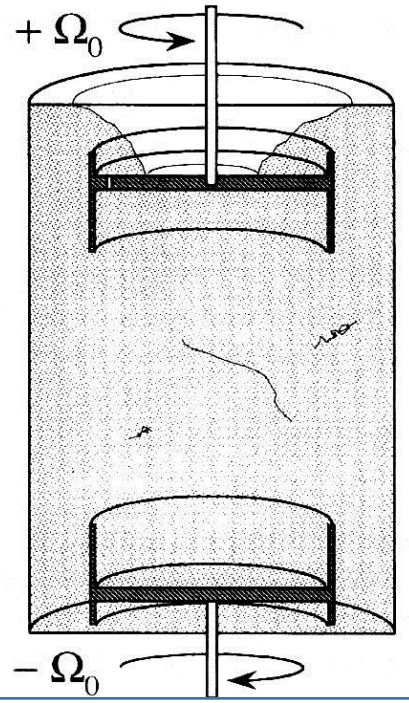

Cavitation in a liquid seeded with bubbles is used as a new visualization technique to single out the region of very low pressure of a fully developed turbulent flow.

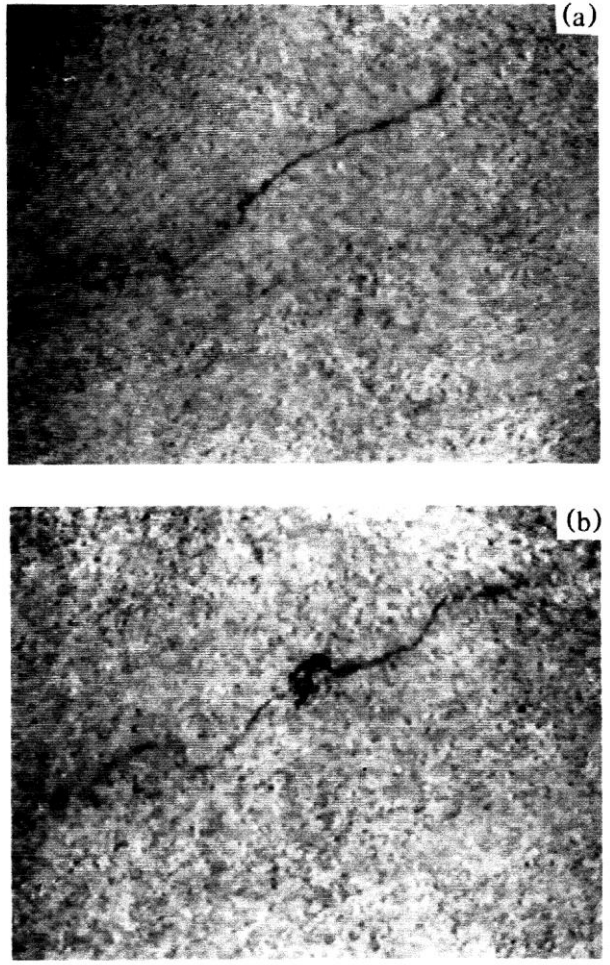

FIG. 2. Detail of two successive video images (taken 0.02 s apart with an exposure time of 0.001 s) showing a side view of a vorticity filament observed in a turbulent flow at a Reynolds number of 80000. Its length is of the order of 5 cm while its diameter (enlarged here by the video image) is of the order of 0.1 mm. (a) The filament at its formation; (b) its destabilization to form kinks.

S.Douady et al., Direct observation of the intermittency of the intense vorticity filaments in turbulence, PRL, vol.67, pp.983-986(1991)

High acceleration event in classical turbulence

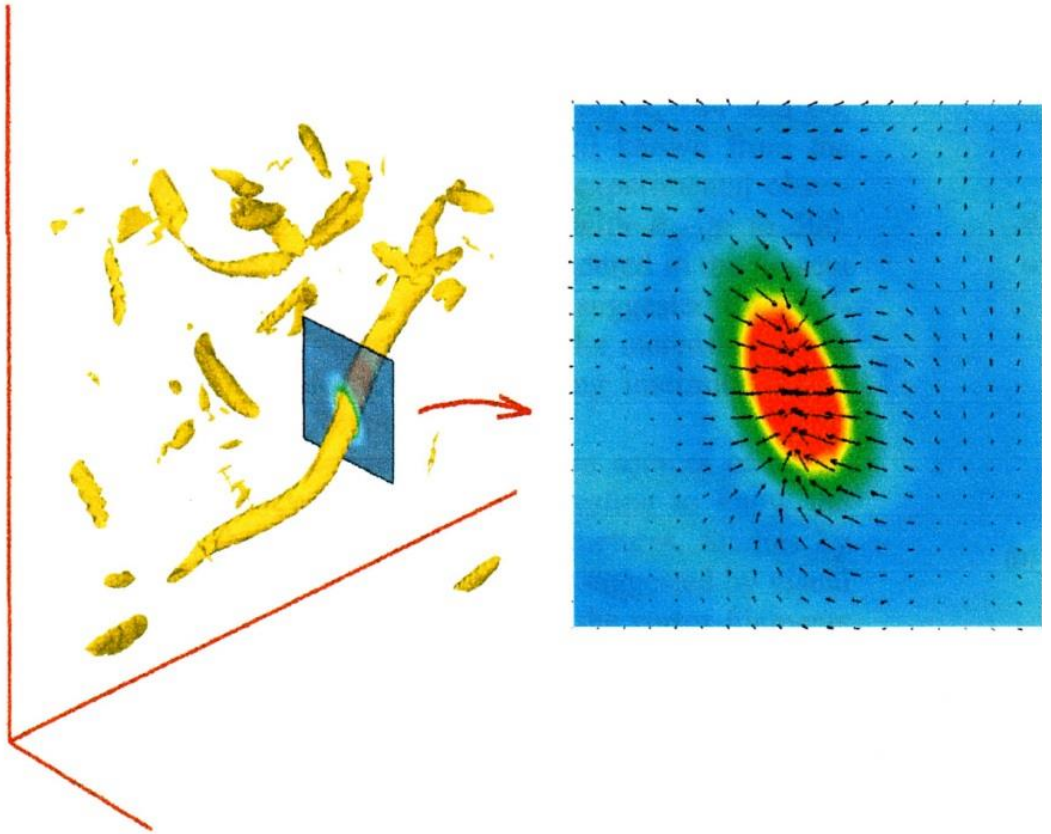

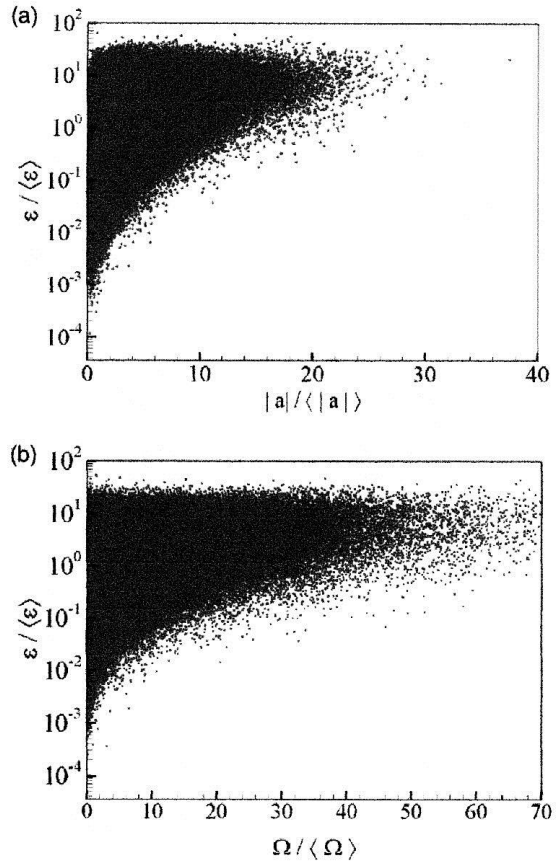

FIG. 4. Correlation plots for (a) $\epsilon - |\mathbf{a}|$ and (b) ϵ-Ω normalized by their own ensemble means. Large acceleration is accompanied by strong dissipation. However, strong dissipation is not always associated with acceleration of large magnitude. ϵ-Ω plot shows a similar trend. However, for $\Omega/\langle\Omega\rangle \sim 20$, ϵ and Ω is uncorrelated in comparison with the same acceleration scale in (a).

S. Lee and C. Lee, Intermittency of acceleration in isotropic turbulence, PRE, vol.71, 056310, (2005)

Instantaneous pressure gradient

wall

$Re_\tau = 180$

$\frac{\partial p}{\partial x}$

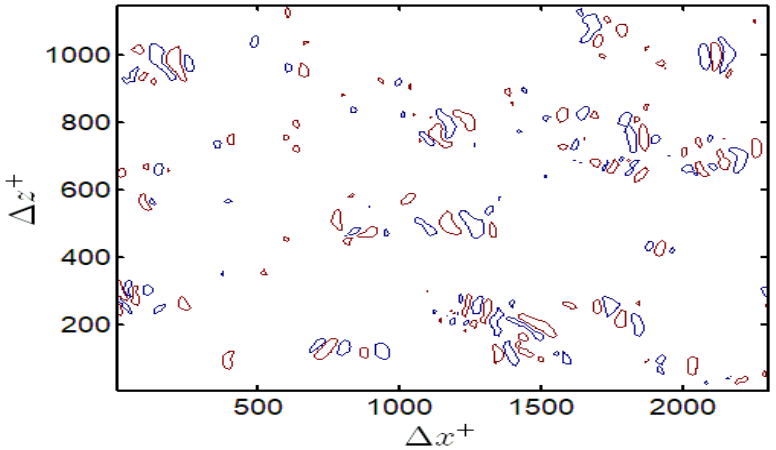

$\frac{\partial p}{\partial y}$

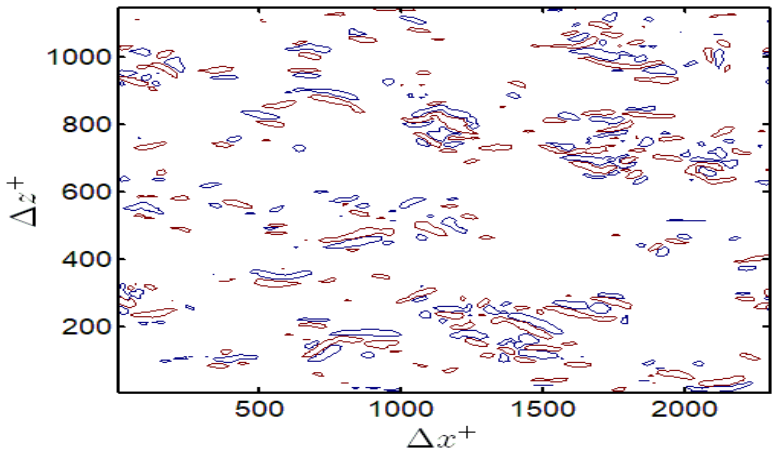

$\frac{\partial p}{\partial z}$

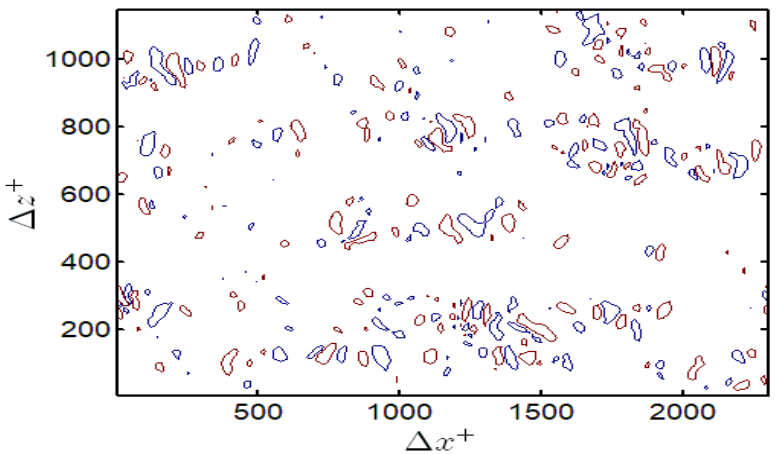

Kim (1989)

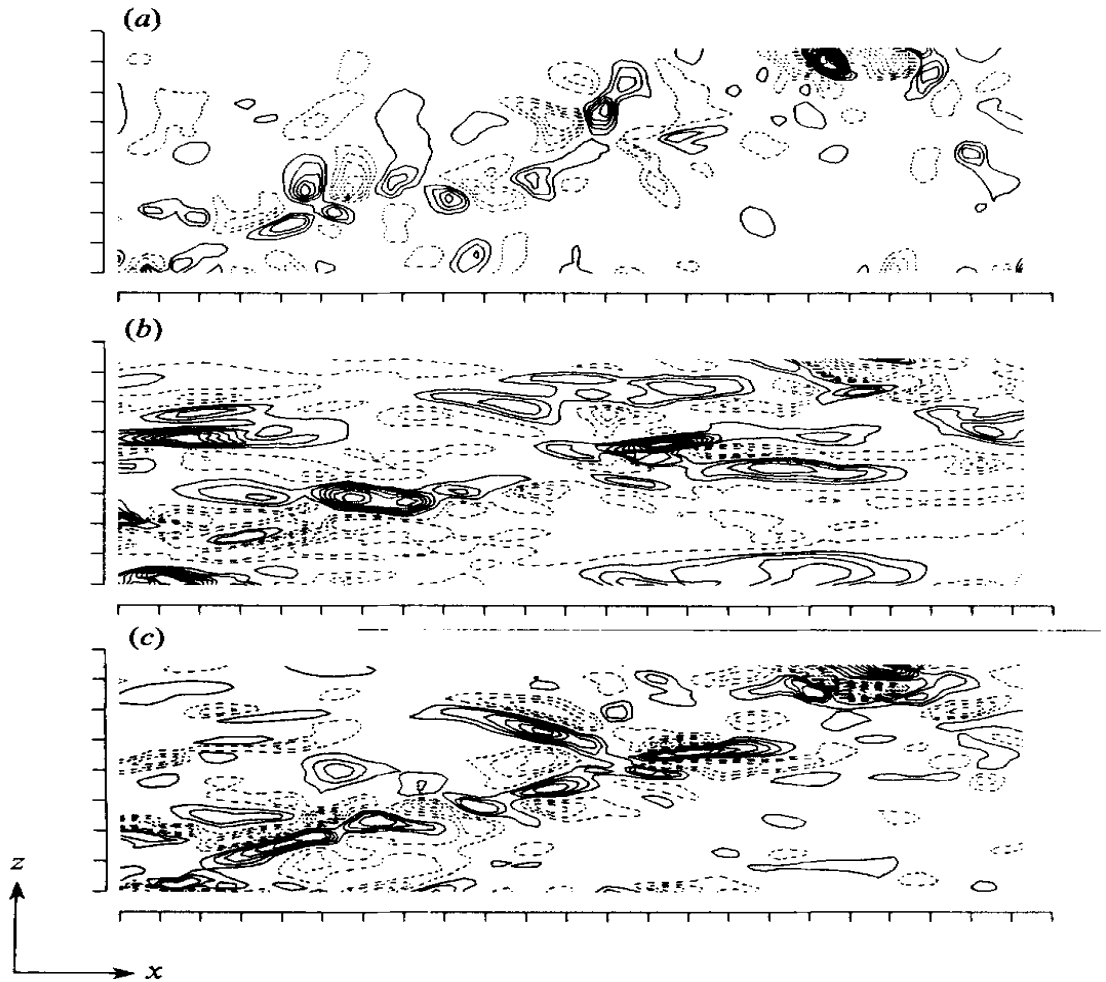

FIGURE 23. Contours of constant (a) $\partial p/\partial x$, (b) $\partial p/\partial y$, and (c) $\partial p/\partial z$ at the wall. The mean flow direction is from left to right, and the tick marks denote 50 wall units.

壁近くの渦構造

渦領域：Q^+>0.02（黒）

変動速度：u^+>3.5（赤），u^+<-3.5（青）

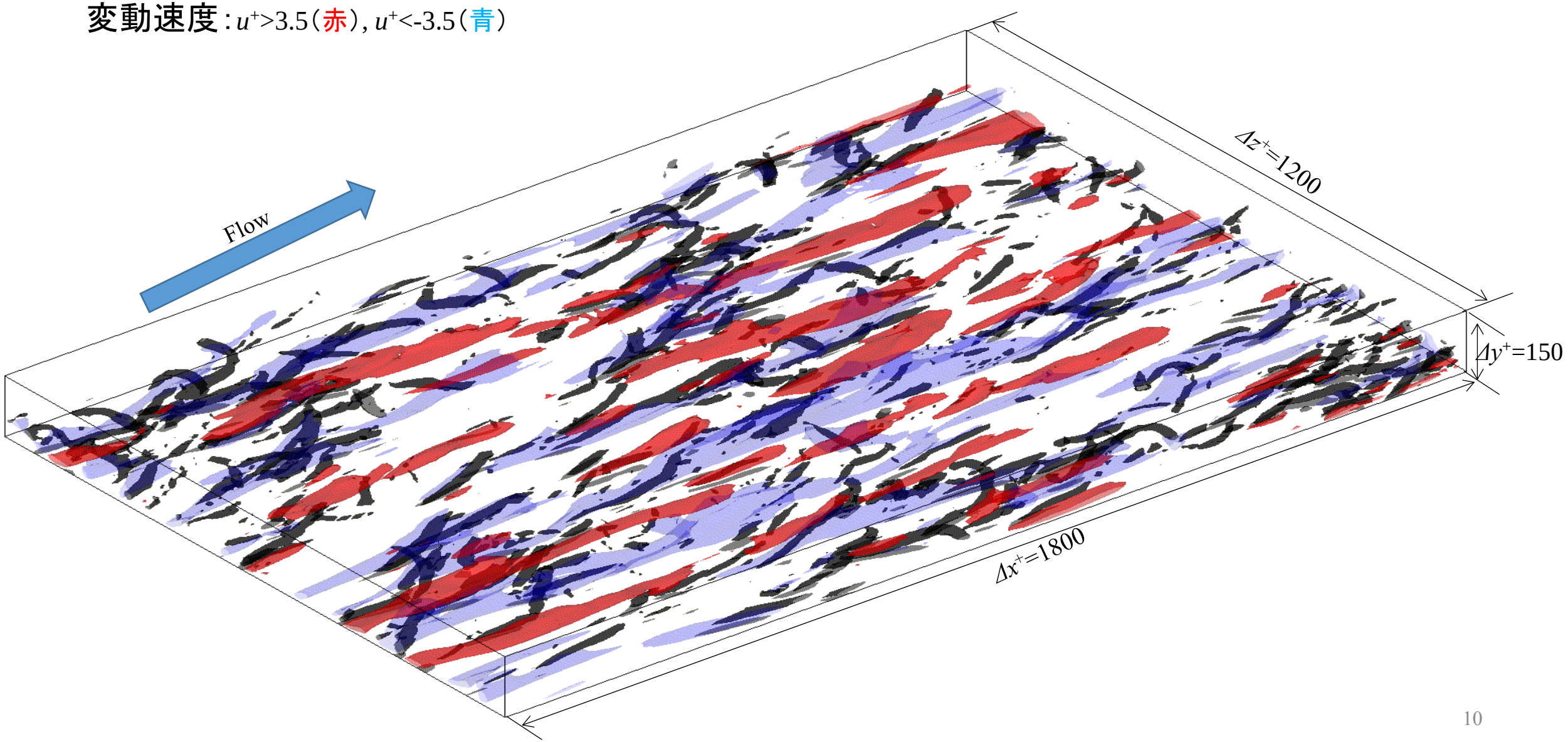

Conditioned pressure gradient

$Re_\tau = 1000$

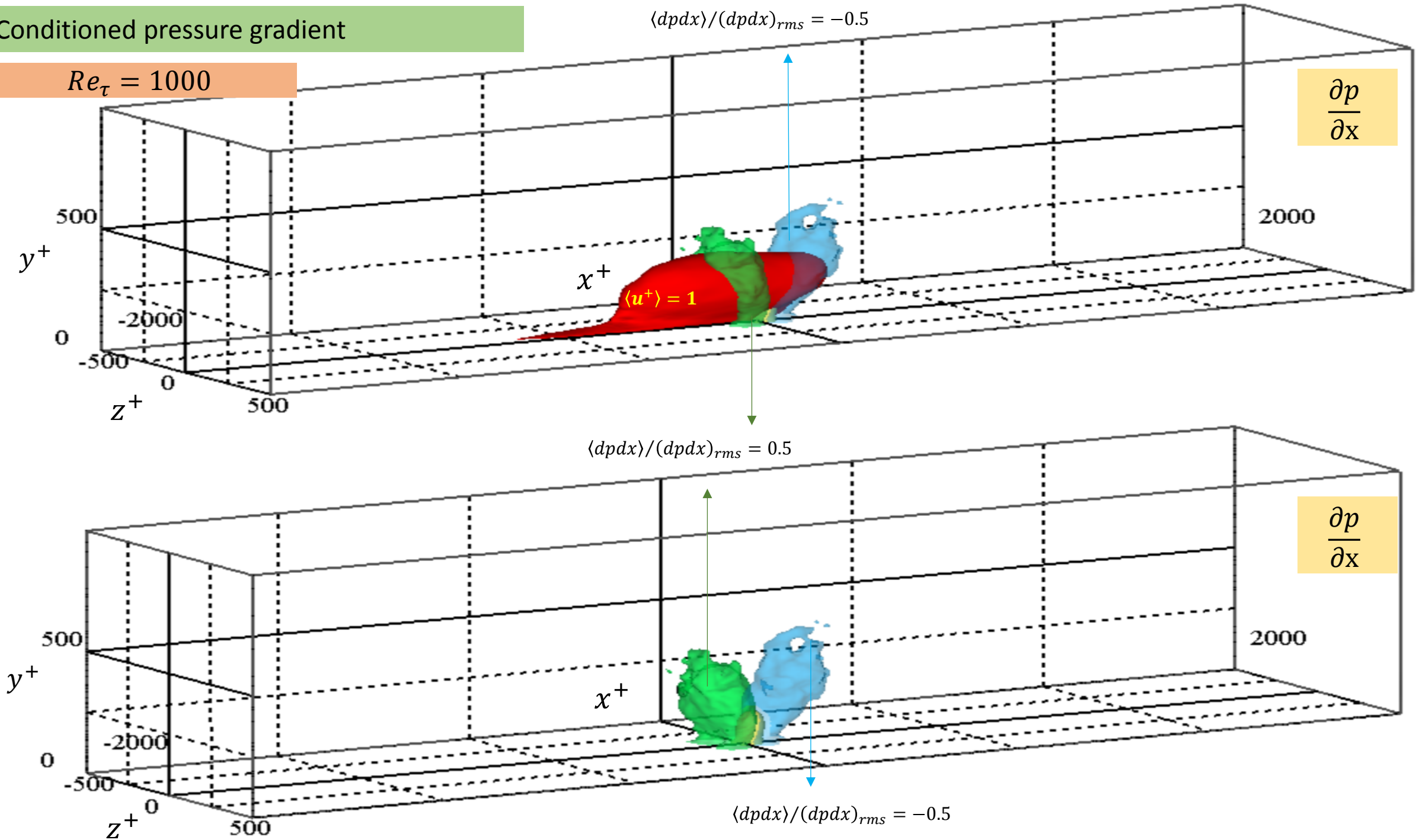

まとめ1

- チャネル乱流の直接数値計算データ（レイノルズ数 から）を解析することから，乱流中の渦構造の壁面圧力との関連を調べた．乱流渦構造は，その中心部で圧力が極小値をとることから，圧力勾配すなわち粒子加速度が大きな値を示す．**乱流構造の時間空間的な間欠分布が，流体粒子加速度の間欠性と密接に関連していると考えられる**．
- 乱流構造の抽出をおこなうために，壁面圧力の大きな変動に注目して，その符号（正と負）で区別した場合の条件付き平均をおこなった．正の壁面圧力は，速度せん断層と密接に関連していること，また，外層からの高速流体の吹込みが寄与する割合が大きい．一方，負の圧力変動は**微細な渦構造**と関連しており，それらの構造は内層変数で無次元化した場合には，Re数の依存性は小さい．
- 今後は，流体粒子加速度の間欠性が渦構造と関連することをより定量的に調べ，壁近くの非等方な流れ場での特徴を明らかにしたい．

Linear Response Analysis

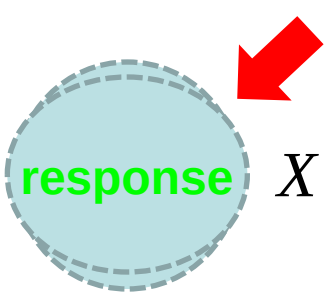

disturbance J

X

Mean velocity gradient
Solid wall effect

equilibrium state

Inertial range

$$X = JX$$

J reflects the physics of thermal equilibrium state

Shear effect on pressure

According to the formula presented by *Ishihara, Yoshioda and Kaneda PRL(vol.88,154501,2002)*, ***pressure*** spectrum is defined by

$$Q_p(\vec{k},t) \equiv \frac{1}{(2\pi)^3}\int d\vec{r}\left\langle p(\vec{x}+\vec{r},t)p(\vec{x},t)\right\rangle e^{-i\vec{k}\cdot\vec{r}}$$

$$Q_p(\vec{k},t) = Q_p{}^0(\vec{k},t) + \Delta Q_p(\vec{k},t)$$

Isotropic part (K41)

$$Q_p{}^0(k) = K_p\varepsilon^{4/3}k^{-13/3}$$

$$\Delta Q_p(\vec{k}) = \alpha\frac{k_1k_2}{k^2}\varepsilon k^{-5}S_{12}$$

$S_{12} = \partial U/\partial y$:Simple mean shear

Modification due to the existence of mean shear.

Anisotropic part

$$\Delta Q_p(\vec{k},t) = C_{mn}(\vec{k})P(k)S_{mn} + C_{ijkl}(\vec{k})R(k)S_{ij}S_{kl}\cdots$$

$C_{mn}(\vec{k})$:2nd order isotropic tensor $C_{ijkl}(\vec{k})$:4th order isotropic tensor

Shear effect on pressure spectrum

IYK formula is well satisfied in this experiment.

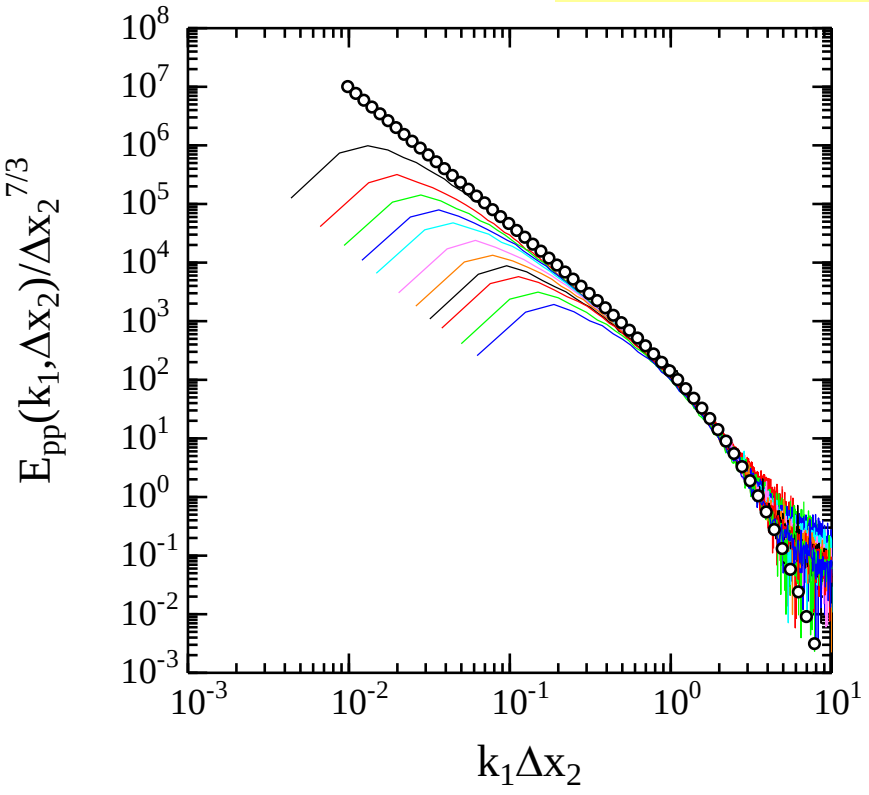

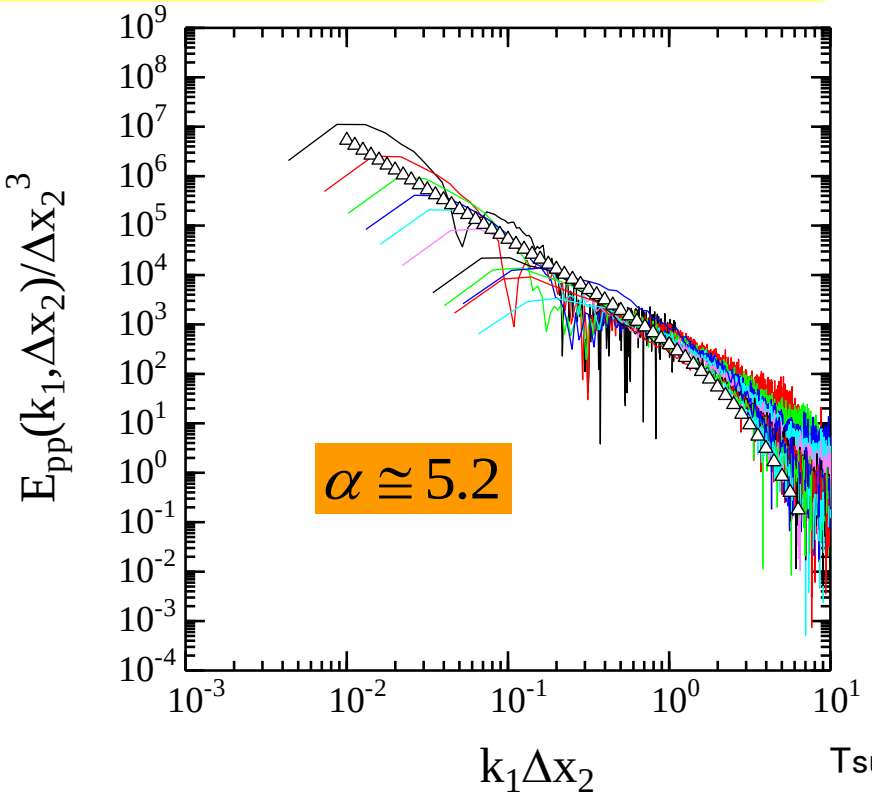

Tsuji&Kaneda JFM(2012)

Isotropic part (K41)

Anisotropic part

$$\frac{E_{pp}(k_1,\Delta x_2)}{\Delta x_2^{7/3}} = K_P\varepsilon^{4/3}(k_1\Delta x_2)^{-7/3} \frac{E_{pp}(k_1,\Delta x_2)}{\sqrt{2}C_1\Delta x_2^{7/3}} = \frac{\Gamma(5/3)}{\sqrt{\pi}\Gamma(7/3)}\left(\frac{k_1\Delta x_2}{2}\right)^{7/6} K_{7/6}(k_1\Delta x_2) + \alpha\varepsilon S_{12}(k_1\Delta x_2)^{-3}\frac{\sqrt{2}C_1}{4\Gamma(5/3)}\frac{d}{d(k_1\Delta x_2)}\left[\left(\frac{k_1\Delta x_2}{2}\right)^{5/2} K_{5/2}(k_1\Delta x_2)\right]$$

Shear effect on acceleration

Similar discussion is possible in case of acceleration $\alpha_i \equiv \partial p / \partial x_i$.

$$E_{\alpha_i\alpha_j}(k) \equiv \sum_{k=|\vec{k}|} \frac{k_i k_j}{k^2} Q_p(\vec{k},t) = \sum_{k=|\vec{k}|} \frac{k_i k_j}{k^2} Q^0{}_p(\vec{k},t) + \sum_{k=|\vec{k}|} \frac{k_i k_j}{k^2} \Delta Q_p(\vec{k},t)$$

Isotropic part (K41)

Anisotropic part

$$E_{\alpha_1\alpha_1}(k_1) = A_1 \varepsilon^{4/3} k_1^{-1/3} + 0 \times \varepsilon k_1^{-3/3} S_{12} + C_1 \varepsilon k_1^{-5/3} S_{12} S_{12}$$

$$E_{\alpha_2\alpha_2}(k_1) = A_2 \varepsilon^{4/3} k_1^{-1/3} + 0 \times \varepsilon k_1^{-3/3} S_{12} + C_2 \varepsilon k_1^{-5/3} S_{12} S_{12}$$

As far as looking for the variance of α_1 and α_2 , there is no significant effect by shear.

$$\langle \alpha_1\alpha_1 \rangle = \int_0^\infty E_{\alpha_1\alpha_1}(k_1) dk_1 \quad \langle \alpha_2\alpha_2 \rangle = \int_0^\infty E_{\alpha_2\alpha_2}(k_1) dk_1 \quad \langle \alpha_1\alpha_2 \rangle = \int_0^\infty E_{\alpha_1\alpha_2}(k_1) dk_1$$

DNS procedures by means of high order accurate Finite Difference Methods

Basic equation Incompressible Navier-Stokes eqs. & continuity eq.

$$\frac{\partial u_i}{\partial x_i} = 0, \qquad \frac{\partial u_i}{\partial t} + u_j \frac{\partial u_i}{\partial x_j} = F\delta_{i1} - \frac{1}{\rho}\frac{\partial p}{\partial x_i} + \nu \frac{\partial^2 u_i}{\partial x_j \partial x_j}.$$

Time integration

Fractional step method with
Euler implicit scheme for pressure term, and 2nd Adams-Bashforth scheme (others)

Spatial discretization

10th order accurate FDM for *x* & *z*,
2nd FDM for *y* on full-staggered grids.

Pressure Poisson eq.

2D-FFT + TDMA(tri-diagonal Matrix Algorithm)

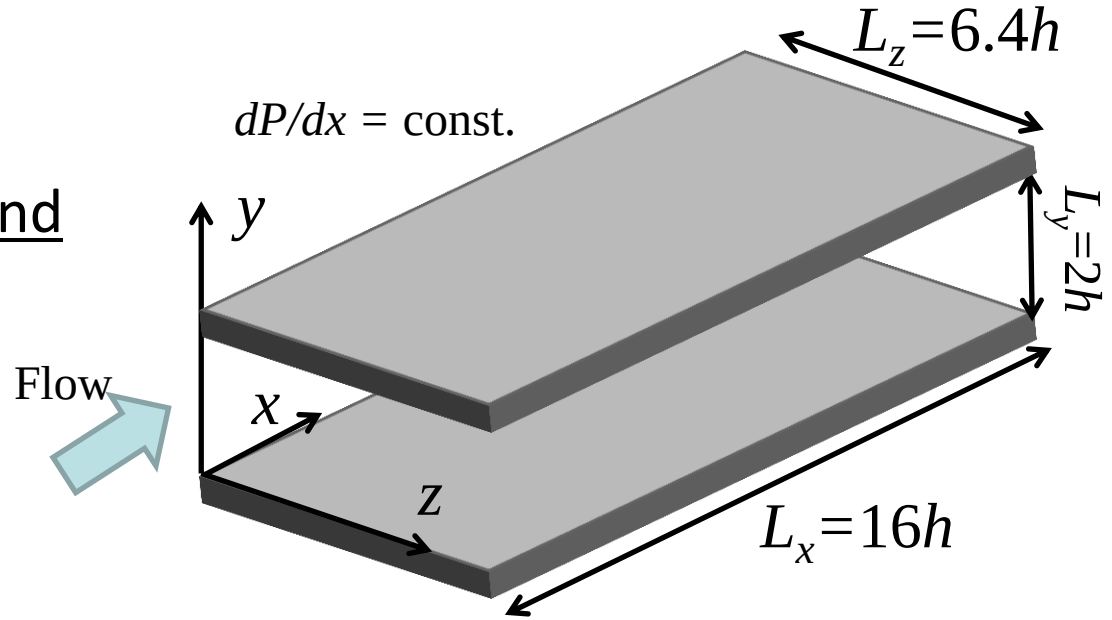

FIG. Configure of turbulent channel flow

Table present DNS conditions

	Re_τ	Δx^+	Δy^+	Δz^+	T^+/Re_τ	U_b^+
10th FDM	1000	11.1	0.3-8.0	8.3	12.0	19.92
10th FDM	2000	11.1	0.3-8.0	8.3	12.6	21.74
10th FDM	4000	11.1	0.3-8.0	8.3	9.0	23.27
10th FDM	8000	14.8	0.3-8.0	8.3	5.2	24.98
Lee & Moser	5186	12.7	0.5-10.3	6.4	7.8	24.10

Statistical convergence

$$E_R = 1 - \frac{y^+}{\mathrm{Re}_\tau} - \left(\frac{dU^+}{dy^+} - \overline{u^+ v^+} \right)$$

In all cases, residual of total shear stress is less than 0.01.

→we considered that stable turbulent statistics were obtained in all cases.

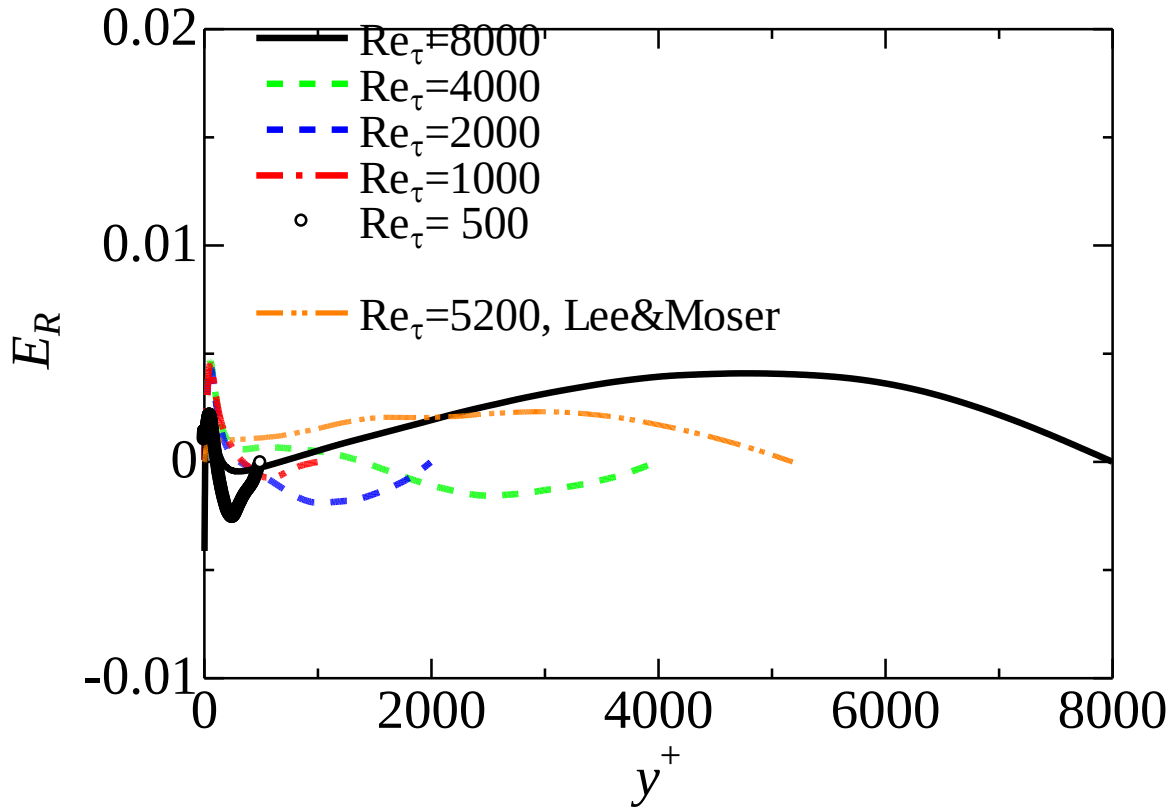

Logarithmic variation of mean velocity

von Kármán constant

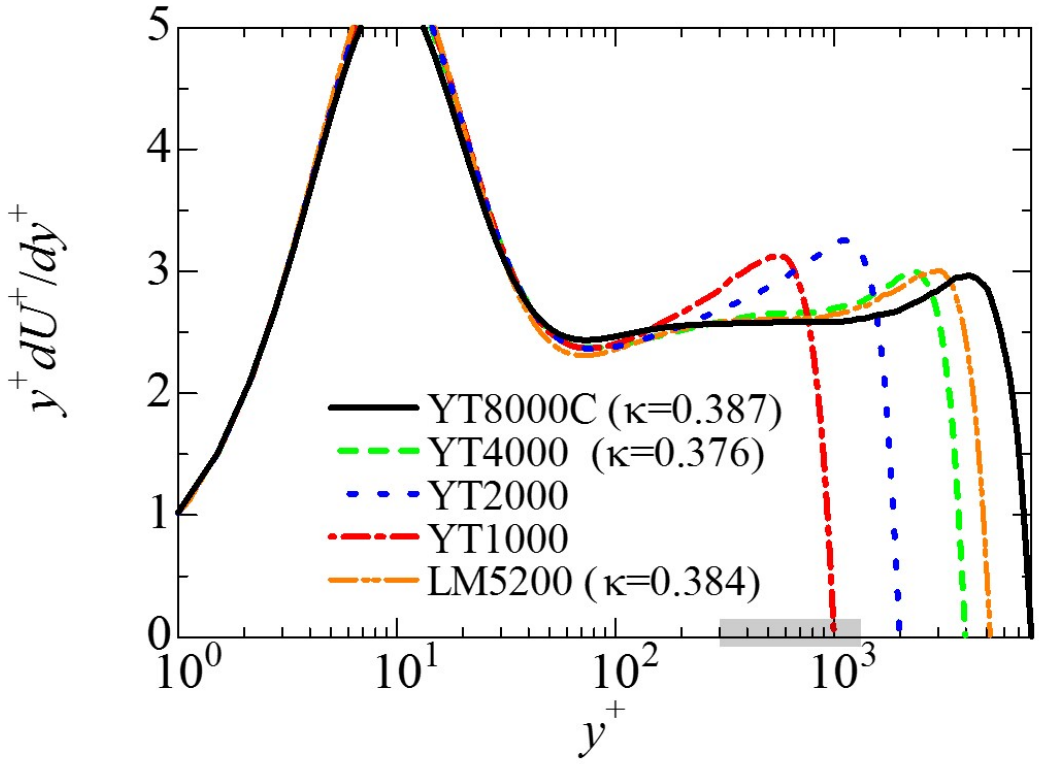

additive constant

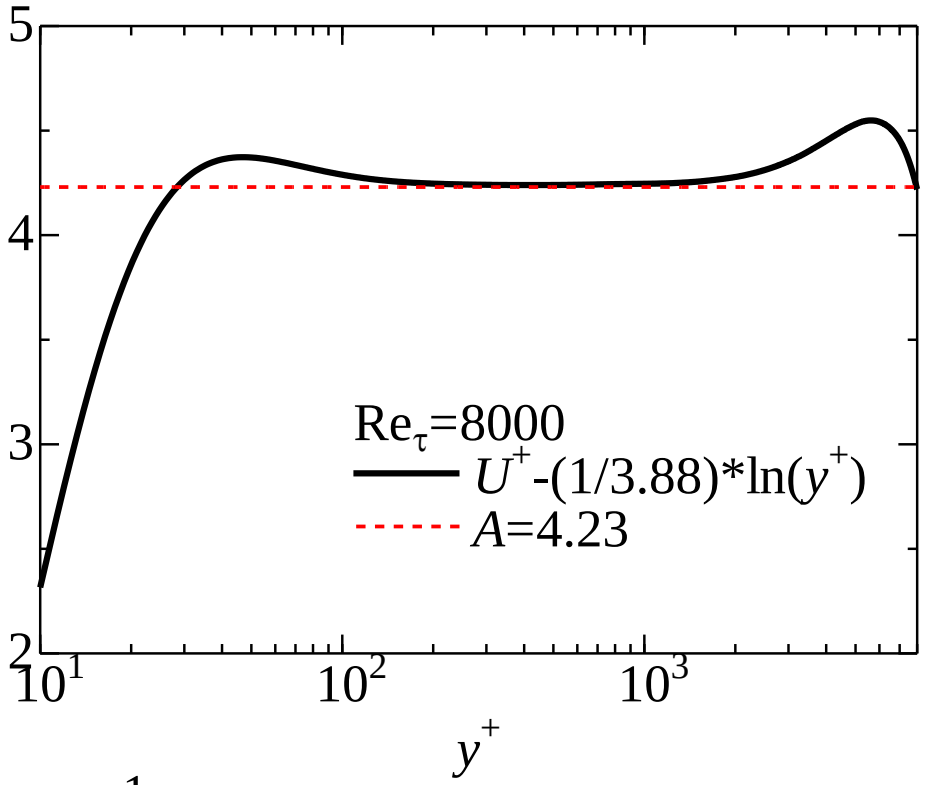

$$U^+ - \frac{1}{\kappa}\ln\left(y^+\right) = B$$

$$U^+ = \frac{1}{\kappa}\ln\left(y^+\right) + B$$

$$\Rightarrow \frac{dU^+}{dy^+} = \frac{1}{\kappa y^+} \quad \therefore \frac{1}{\kappa} = y^+ \frac{dU^+}{dy^+}$$

In Re_τ=8000,
κ= 0.387, B=4.21
between 300 < y^+ < 1100 (y/h =0.14)

Logarithmic variation of streamwise Reynolds stress

von Kármán constant

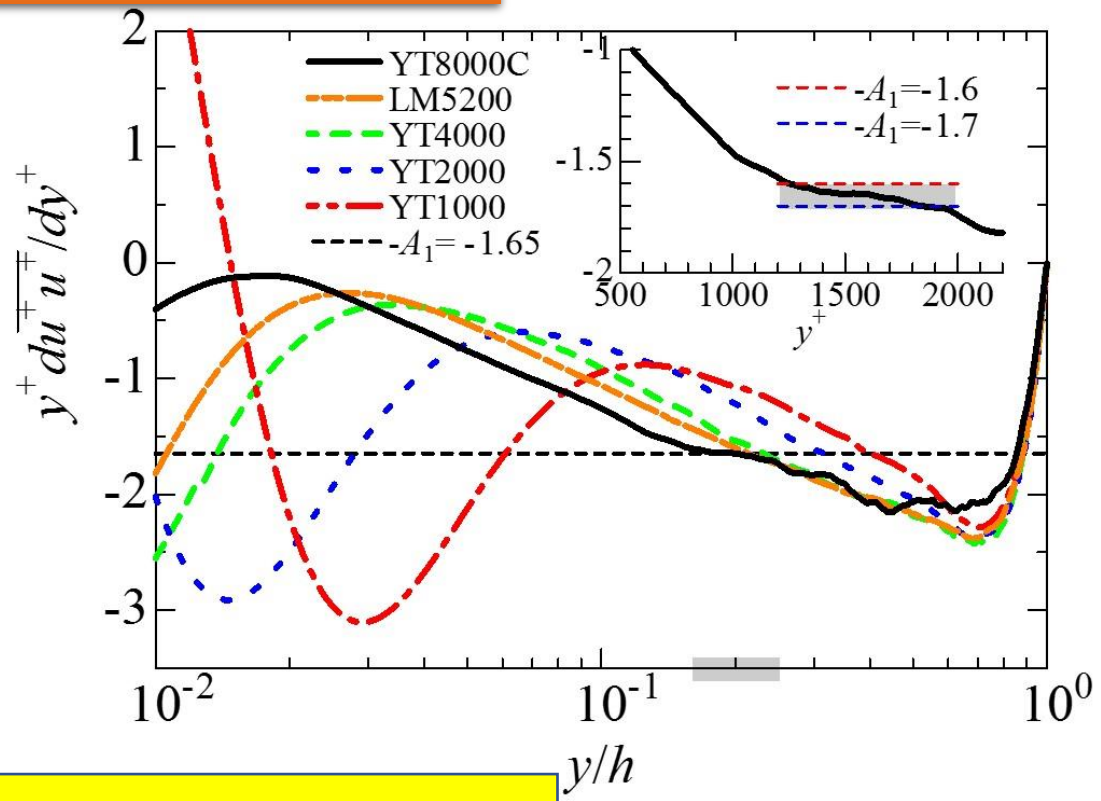

additive constant

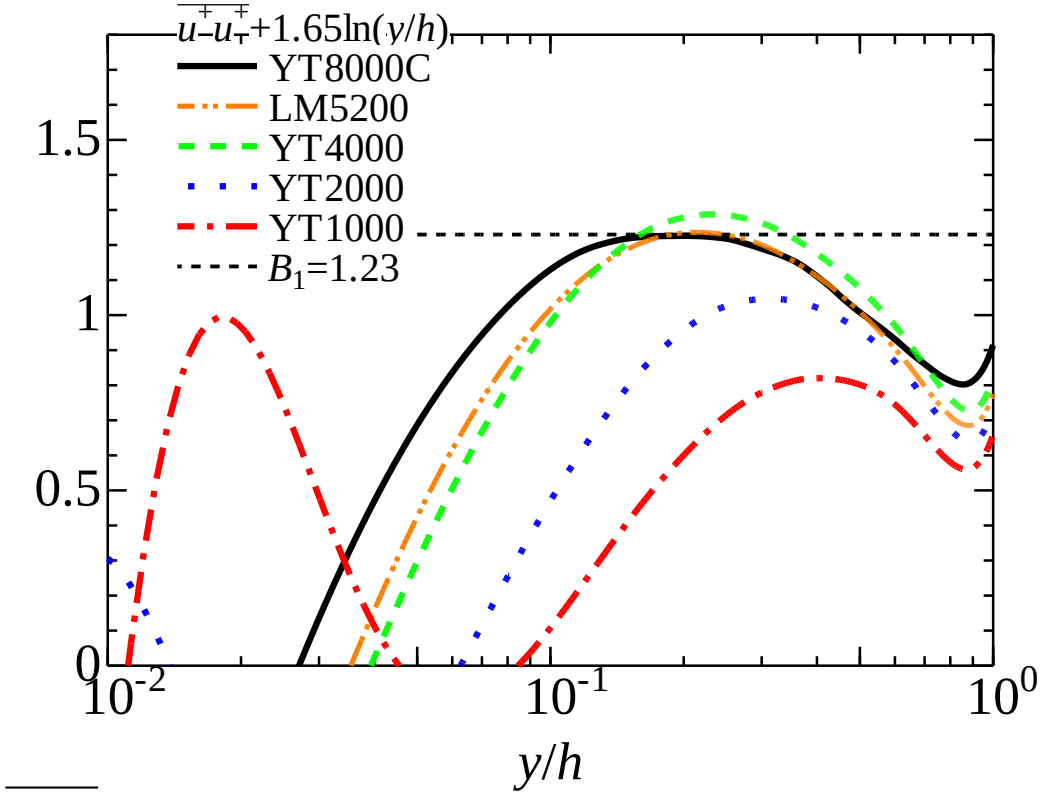

$$\overline{u^+u^+} = B_1 - A_1 \ln(y/h)$$

$$\Rightarrow y^+ \frac{d\overline{u^+u^+}}{dy^+} = -A_1$$

$$\overline{u^+u^+} + A_1 \ln(y/h) = B_1$$

In Re_τ=8000,

A_1= 1.65, B_1=1.23

between 1200(y/h=0.15) < y^+ < 2000 (y/h =0.25)

Comparison with experimental results

$$\overline{u^+u^+} = B_1 - A_1 \ln(y/h)$$

Present :channel (DNS) at Re_τ=8000

A_1= 1.65, B_1=1.23
between 1200(y/h=0.15) < y^+ < 2000 (y/h =0.25)

Marusic et al. JFM(2013)

Facility	A_1	B_1	κ	A
LCC	1.21±0.08	2.20±0.25	0.384*	4.17*
Melbourne	1.26±0.06	2.30±0.18	0.387±0.004	4.32±0.20
Superpipe	1.23±0.05	1.56±0.16	0.391±0.004	4.34±0.19
SLTEST	1.33±0.17	2.14±0.40	0.410±0.028	4.44±1.83

TABLE 2. Parameters in (1.1) and (1.2) obtained from least-squares error curve fit for data in the region $3Re_\tau^{1/2} < z^+ < 0.15Re_\tau$. The uncertainty estimates are based on 95% confidence bounds from the curve-fitting procedure. An asterisk denotes values where a composite formulation was used to determine U_τ with these assumed constants.

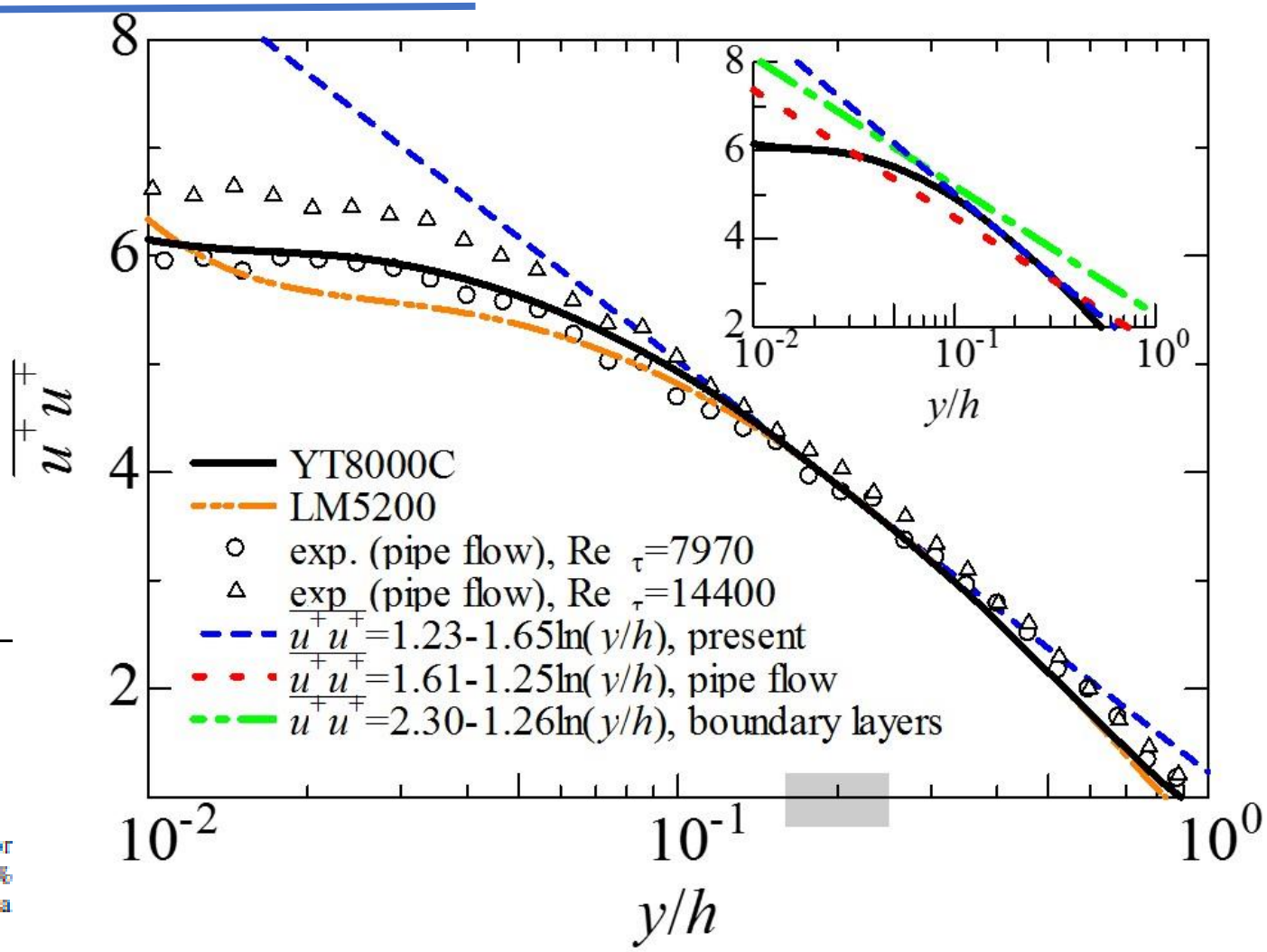

The log-region in channel at Re_τ=8000 is located around $y/h \approx 0.2$. By contrast Hultmark et al. PRL(2012) and Marusic et al. JFM(2013) reported that the log-regions are located around $y/h \approx 0.1$.

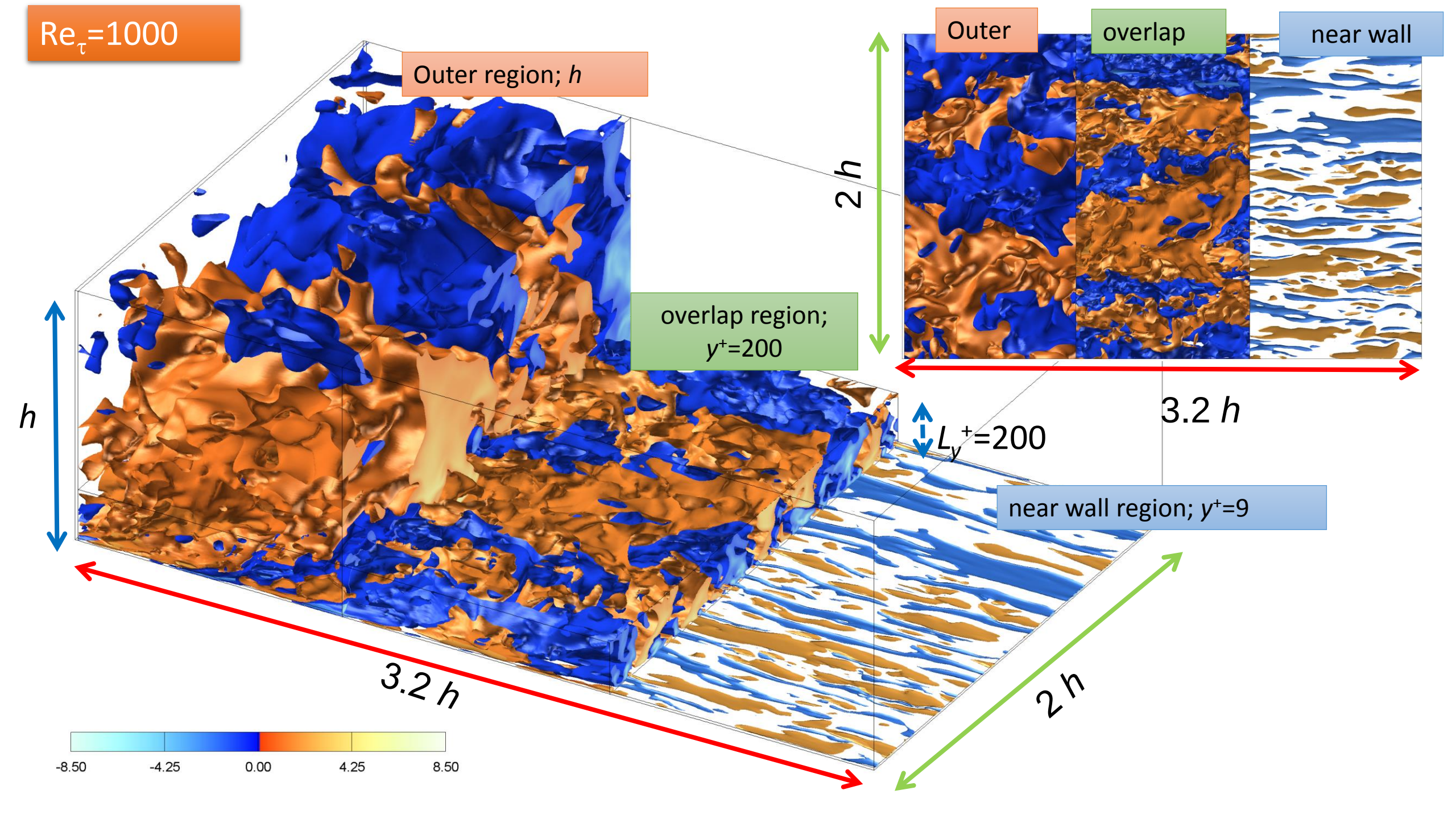
Re$_\tau$=1000
Outer region; h
overlap region; y^+=200
near wall region; y^+=9
Outer
overlap
near wall
2 h
h
3.2 h
L_y^+=200
3.2 h
2 h
-8.50
-4.25
0.00
4.25
8.50

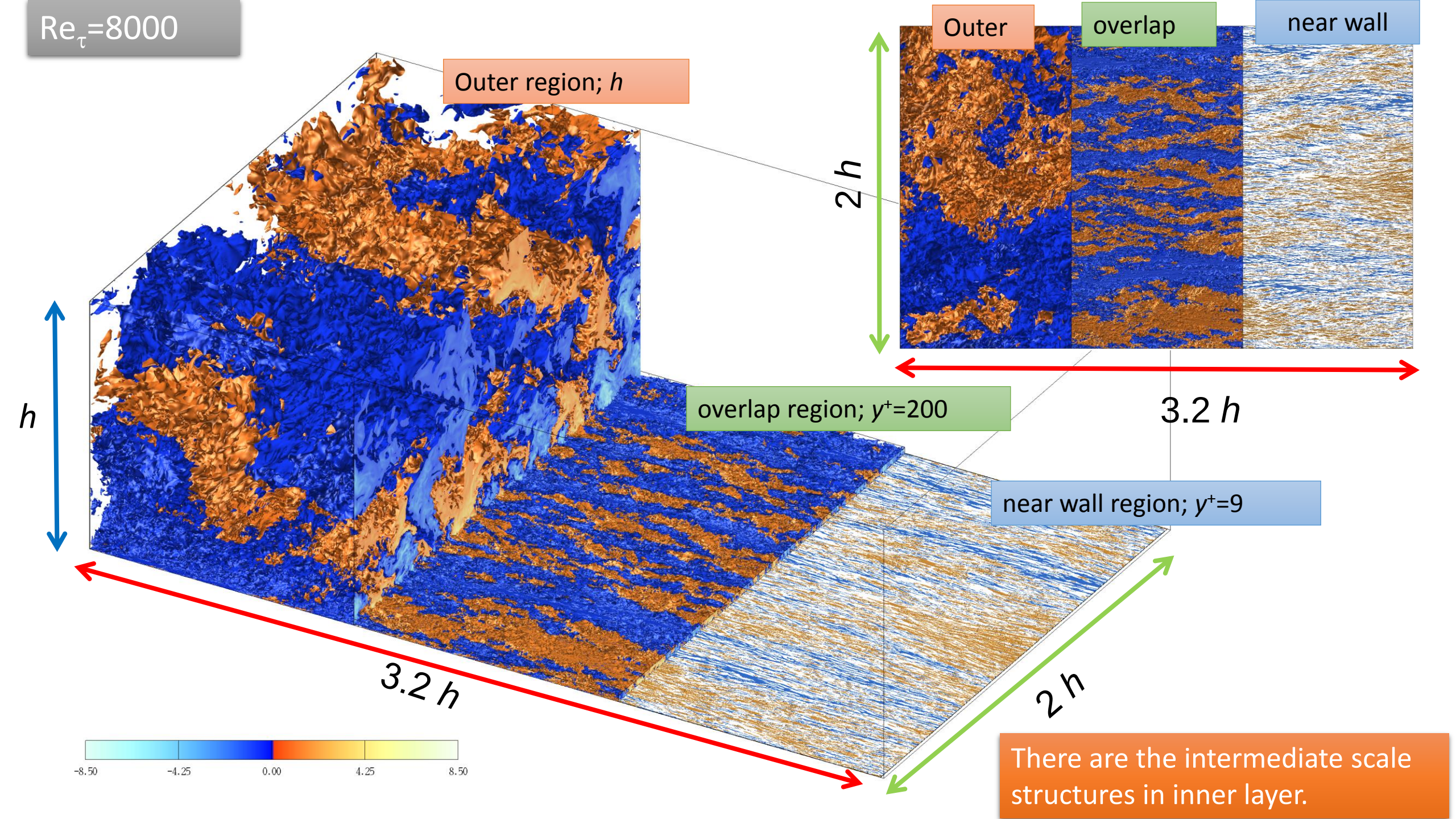
Re_τ=8000
Outer region; h
overlap region; y^+=200
near wall region; y^+=9
Outer
overlap
near wall
2 h
h
3.2 h
3.2 h
2 h
-8.50
-4.25
0.00
4.25
8.50
There are the intermediate scale structures in inner layer.

High-Reynolds number researches in Japan

Recent high Reynolds number researches in wall-bounded turbulent shear flow are studied for investigating the universal feature of mean velocity and turbulence intensity profiles in canonical shear flows.

Yamamot&Tsuji, Numerical evidence of logarithmic regions in channel flow at $Re\tau$ = 8000,PRF 3, 012602(R) (2018) — Channel flow

Furuichi et al, Friction factor and mean velocity profile for pipe flow at high Reynolds numbers, Physics of Fluids 27, 095108 (2015)
Furuichi et al, Further experiments for mean velocity profile of pipe flow at high Reynolds number, submitting (2018) — Pipe flow

Boundary layer flow

Do the mean velocity and turbulence intensity profiles show log-law profile in high-Re number ? Are they universal ?

$$U^+ = \frac{1}{\kappa}\log(y^+)+\mathrm{B}$$

Where is log-region? What are the values of κ and B ?

$$(u^+_{rms})^2 = A_1\log(y^+)+B_1$$

Where is log-region? What are the values of A_1 and B_1 ?

→ 大気乱流場へ

κ= 0.387, B=4.21

A_1= 1.65, B_1=1.23

Importance of high-Reynolds number flows

- Turbulent flows with $Re_\tau >> O(10^3)$ are of interest because this is the range of Reynolds number relevant to industrial applications.
- **high-Re characteristics in wall-bounded flows**

- Logarithmic variation of mean velocity was evident at **Re_τ = 5200**, Lee & Moser, JFM(2015), channel(DNS)
- Appearance of two distinct energy peaks in the premultiplied streamwise velocity spectra, at **Re_τ >4000**, Hutchins et al. JFM(2009), boundary layer(exp.)
- k_x^{-1} law was only evident at **Re_τ >5250**, Nickel et al. PRL(2006), boundary layer(exp.)
- Logarithmic variation of streamwise Reynolds stress was evident at **Re_τ >20000**, Marusic et al. JFM(2013), exp.

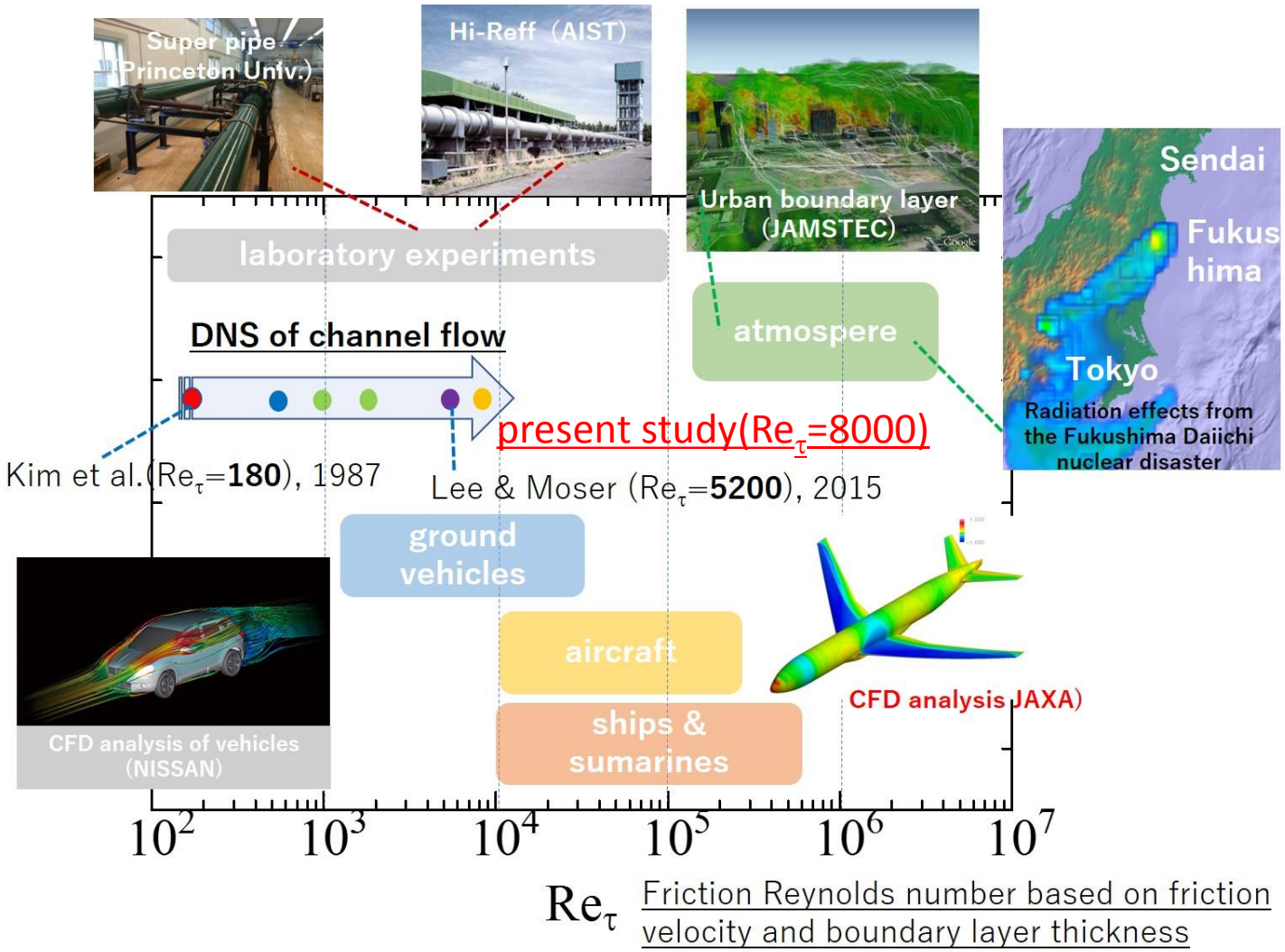

FIG.1 Typical Reynolds numbers in wall-turbulence applications based in Deck et al. (2014)